PAPER

Check for updates

A 2,6-diamidopyridine-based macrocyclic aromatic amide receptor with cascade ion pair recognition†

Xinguo Mao,[a] Rui Zhang, [ID] [a] Yulong Sun,[d] Xuping Wang, [ID] *[a] Qinggang Li,[a] Han Zuilhof, [ID] *[b] Leyong Wang [ID] [c] and Qiang Shi [ID] *[a]

Ion-pair receptors constitute an important class of synthetic receptors within the realm of host–guest and supramolecular chemistry. Their unique ability to simultaneously recognize and accommodate both cations and anions has rendered them invaluable across various applications. In this study, we have synthesized a cascade macrocyclic ion-pair receptor, composed of three 2,6-amidopyridine building blocks bridged by aromatic spacers. Notably, the diamide binding sites of this receptor exhibit a high degree of selectivity for fluoride ions. Furthermore, despite lacking any dedicated cation-binding sites within its macrocyclic structure, this receptor is capable of selectively binding tetraethylammonium cations through a series of cascade electrostatic interactions facilitated by the bound flouride ions.

Introduction

Artificial macrocyclic receptors stand as the cornerstone of supramolecular chemistry,[1] featuring pre-organized cyclic skeletons and central cavities. Typically, these receptors are constructed from fundamental building blocks, which serve as the basic structural units within a symmetric molecular host.[2] The intrinsic properties, recognition capabilities, and diverse applications[3,4] of these macrocycles are largely dictated by the composition of these building blocks. For instance, the electron-dense *p*-dimethoxybenzene constitutes the backbone of pillar[*n*]arenes (*n* = 5, 6), enabling their cavities to host electron-deficient guests like ammonium or pyridinium salts.[5–7] Conversely, the blue box, employing paraquat as its foundational unit, possesses an electron-deficient cavity tailored for recognizing electron-rich guests.[8] Thanks to the variety of building blocks, a plenty of artificial macrocyclic receptors have been synthesized and investigated.[9–12]

Traditionally, macrocycles have predominantly been designed as monotopic receptors, tailored to bind specific guest species. In contrast, ion-pair receptors[13–17] exhibit a unique ability to simultaneously capture both cations and anions. To date, two primary types of ion-pair receptors have been devised: heterotopic[18,19] and cascade[13] receptors. Heterotopic receptors integrate anion and cationic recognition sites within a single macrocyclic skeleton, whereas cascade receptors could host ion pairs through relay interactions like the form of [H···A$^{-(+)}$··· B$^{+(-)}$], whereas H is the cascade macrocyclic receptor with only binding sites for A$^{-(+)}$ guest, B$^{+(-)}$ guest is attracted by encapsulated A$^{-(+)}$ counterion through noncovalent interactions of them such as electrostatic interaction, rather than weak interactions with the macrocycle. The recognition mechanism endows ion-pair receptors with enhanced selectivity for separating specific cations and anions.[20,21] Consequently, ion-pair receptors, particularly heterotopic ones, are garnering significant attention due to their promising applications in salt extraction,[22] membrane transport,[23,24] sensing,[25] and beyond.[26] Currently, there is a surge of research focusing on the design, synthesis, and functionality of these receptors. However, cascade ion-pair receptors, despite their advantages of straightforward design, easy synthesis and broader applicability, have received comparatively less attention.[27]

Amide, a ubiquitous and versatile building block, finds extensive use not only in polypeptides and proteins but also in artificial macrocycles,[28] owing to its exceptional properties as a hydrogen bonding donor or acceptor. 2,6-Diamidopyridine, a distinctive diamide fragment, adopts a predominantly fixed V-shape conformation due to intramolecular hydrogen bonding between the pyridine ring's nitrogen atom and the amide group's hydrogen atoms.[29] This conformation enables it to function as a chelating hydrogen bond donor, capturing hydrogen bond acceptor molecules such as anions.[30] Furthermore, 2,6-diamidopyridine has been established as a ligand for certain transition metal complexes.[31,32] Leveraging its

[a]Key Laboratory of Light Conversion Materials and Technology, Shandong Provincial Key Laboratory of High Strength Light Weight Metallic Materials, Advanced Materials Institute, Qilu University of Technology (Shandong Academy of Sciences), Jinan, 250014, China. E-mail: shiqiang@sdas.org; wangxp@sdas.org

[b]Laboratory of Organic Chemistry, Wageningen University, Stippeneng 4, 6708 WE Wageningen, The Netherlands. E-mail: Han.Zuilhof@wur.nl

[c]Key Laboratory of Mesoscopic Chemistry of MOE, School of Chemistry and Chemical Engineering, Nanjing University, Nanjing, 210023, China

[d]Shigatse Science and Technology Bureau, Shigatse, Tibet, 857000, China

† Electronic supplementary information (ESI) available: ^{1}H NMR and ^{13}C NMR of compounds, as well as the details of the experiments. See DOI: https://doi.org/10.1039/d5ra00434a

directional hydrogen bonding sites, derivatives of 2,6-dia-midopyridine emerge as exceptional building blocks for constructing macrocyclic receptors capable of capturing anionic guests.[33,34]

In this study, capitalizing on the 120° angle formed by the two amide groups in 2,6-diamidopyridine derivatives, we report herein the synthesis of a novel class of hexagonal macrocyclic aromatic amide (**MAA**, Fig. 1), interlinked by aromatic spacers. This macrocycle, equipped with three diamide binding sites, demonstrated remarkable selectivity for fluoride ions[35,36] and formed a cascade complex with tetraethylammonium cations upon fluoride binding, without requiring any cationic binding sites within the macrocyclic structure.

Results and discussion

Macrocycle synthesis

The synthetic route of macrocyclic aromatic amide receptor **MAA** was shown in Scheme 1. The intermediate meso-triphenylenediamine derivative **1** was first efficiently synthesized from 1,3-dibromo-5-methoxybenzene and 2 equivalents of 4-(4,4,5,5-tetramethyl-1,3,2-dioxaborolan-2-yl) aniline by a Suzuki–Miyaura coupling reaction (86% yield, typically 4.86 mmol scale). In this experiment, a mixed solvent system of 1,4-dioxane and H_2O was used to facilitate the complete dissolution of the reactants and the separation of the product. Next, **MAA** was prepared by the condensation reaction of intermediate **1** with equal equivalents of 2,6-pyridinedicarboxylic acid in THF using EDC and HOBT as condensation reagents (typical yield *ca.* 5% on 8×10^{-2} mmol scale). In this study, the two molecules, **1** and 2,6-pyridinedicarboxylic acid, were chosen as the fragments for the synthesis of **MAA** because they had the precisely right bond angles to allow the 3 + 3 amide condensation to form an amide macrocycle with three pyridines and three diamides. Compared with some low polar solvents such as dichloromethane (DCM), the use of THF as the reaction solvent improved both the solubility of the reactants and the yield of **MAA**. Meanwhile, it should be noted that some precipitate was produced during the reaction, which likely was due to the formation of non-cyclic oligomers and polymers. After **MAA** was isolated using column chromatography, recrystallizations were performed to further improve the purity of the product. All
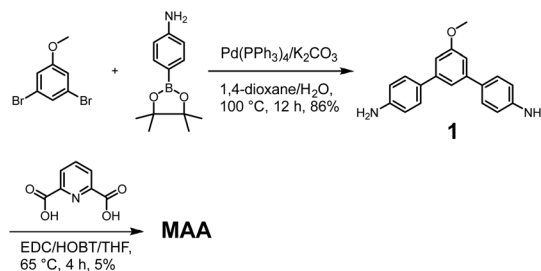
Scheme 1 Synthetic route towards **MAA**.

products were characterized by ^{1}H NMR, ^{13}C NMR and HRMS (Fig. S1 to S4†).

Recognition ability and selectivity to anions

In order to investigate the recognition properties of **MAA**, equal amounts (2.97×10^{-2} M) of different species of $Et_4N^+X^-$ ($X^- = F^-$, Cl^-, Br^-, I^-, HSO_4^-, $CF_3SO_3^-$) were, in separate experiments, added to a DMSO-d_6 solution of acceptor **MAA** at 298 K, and the changes in the ^{1}H NMR spectrum observed (Fig. 2). Upon the addition of the F^- salt, the ^{1}H NMR spectra showed obvious chemical shifts. Most strongly, the amide $-(C=O)N–H$ proton peak showed a large downfield shift from 11.2 to 14.8 ppm (more precisely: $\Delta\delta = 3.68$ ppm). In addition, the ^{1}H peaks in the aromatic region also changed significantly, with partial overlapping of the A, B peaks shifted upfield (A: $\Delta\delta = -0.13$ ppm; B: $\Delta\delta = -0.18$ ppm and the D peak shifted to downfield ($\Delta\delta = 0.29$ ppm). Smaller, but still significant changes were observed for the C, E, and F peaks, which also showed upfield shifts ($\Delta\delta = -0.15$ ppm, -0.08 ppm, and -0.07 ppm, respectively). The results clearly demonstrated the formation of stable complexes of **MAA** with F^- in DMSO-d_6. In sharp contrast, the addition of anions such as Cl^-, Br^-, I^-,
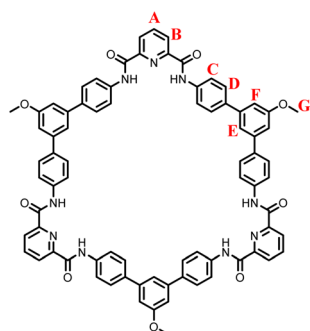

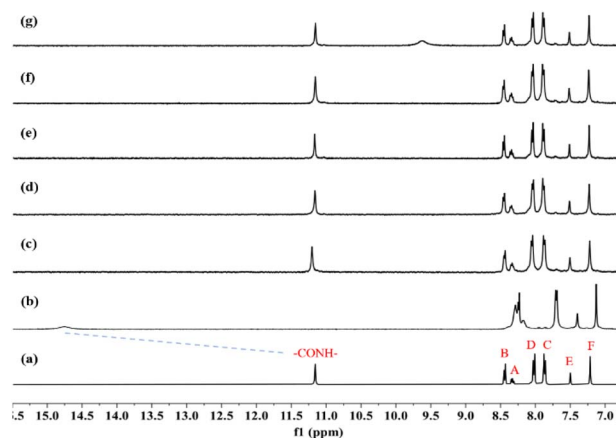**Fig. 1** Structure of the macrocyclic aromatic amide (**MAA**) receptor.

Fig. 2 ^{1}H NMR (400 MHz, DMSO-d_6, 298 K) of (a) receptor **MAA**; (b) **MAA** + 5.0 equiv. of tetraethylammonium fluoride; (c) **MAA** + 5.0 equiv. of tetraethylammonium chloride; (d) **MAA** + 5.0 equiv. of tetraethylammonium bromide; (e) **MAA** + 5.0 equiv. of tetraethylammonium iodide; (f) **MAA** + 5.0 equiv. of tetraethylammonium trifluoromethanesulfonate; (g) **MAA** + 5.0 equiv. of tetraethylammonium hydrogensulfate.

HSO_4^-, and $CF_3SO_3^-$ hardly induced any significant chemical shifts in the ^1H NMR spectrum of **MAA**. This indicates the absence of any significant complex formation in DMSO-d_6 of **MAA** with these anions, and thus a remarkably strong and selective binding of fluoride to **MAA**. In addition, the binding ratio of **MAA** with F^- was detected to 1 : 2 (Fig. S5 and S6†).

In order to quantify the complexation ability of the receptor **MAA** to F^-, ^1H NMR titration experiments were carried out (DMSO-d_6, 298 K; Fig. S7†), in which F^- was added to **MAA** and the step sized changes in the corresponding ^1H peaks observed. Based on these NMR titration data, the **MAA** and F^- binding constants could be calculated by the nonlinear curve fitting method (Fig. S8†), which were $K_{a1} = (1.47 \pm 0.40) \times 10^4 \ M^{-1}$ and $K_{a2} = (7.15 \pm 0.51) \times 10^3 \ M^{-1}$, respectively.

UV-vis spectrophotometric studies

During the study of recognition studies of receptor **MAA** with the tetraethylammonium salts of F^-, Cl^-, Br^-, I^-, HSO_4^- and $CF_3SO_3^-$, it was found that after the addition of tetraethylammonium fluoride (Et_4NF) to the DMSO solution of **MAA**, a drastic color change from colorless to yellow could be observed by the naked eye. In contrast, the addition of several other anions did not result in any noticeable color change, as shown in Fig. 3. This distinct color change also reflected the highly selective recognition of F^- by receptor **MAA**, making it useful for rapid detection and recognition of F^-.

In order to further investigate the phenomenon of color change after the addition of F^-, UV-vis spectrophotometric experiments were carried out in a DMSO solution of **MAA** (1.98 $\times 10^{-4}$ M). Fig. 4 shows the UV-vis absorption spectra after the addition of 5 equivalents of the selected anions, all of which resulted in an increase in the absorption intensity in the visible band due to the fact that the selected anions all carry lone pairs of electrons, which acted as a color-booster in the UV-vis spectrophotometric experiments. However, after the addition of F^-, the UV-vis absorption spectrum of **MAA** not only showed an increase in absorbance, but also an obviously redshift maximum ($\Delta\lambda = 8$ nm) and a new shoulder peak formed at 367 nm which correspond to the deprotonation[37] of –NH– groups by F^- ions (Fig. S10†). Combined with the chemical shift changes of the –CONH– group and the peaks of the aromatic region upon the addition of F^- (Fig. 2), this further indicates the

Fig. 4 UV-vis absorption spectra of **MAA** (in DMSO) to which various salts was added.

formation of a stable complex between **MAA** and F^- in DMSO solution.

Selective ion-pair recognition

As shown in Fig. 5, it was found from ^1H NMR that there were different binding patterns of **MAA** with different cations including smaller tetraethylammonium cation (Et_4N^+) and larger tetrabutylammonium ion (n-Bu_4N^+). The addition of the receptor **MAA** to the solution of Et_4NF resulted in a pronounced upfield shift (CH_2 peak: $\Delta\delta = 0.04$ ppm; CH_3 peak: $\Delta\delta = 0.02$ ppm) of Et_4N^+ as shown in (b) and (c) in Fig. 5, implying that the small Et_4N^+ has "fallen into" the cavity of the complex of **MAA** with F^- ions, and therefore the formation of ternary complex between **MAA** with two F^- ions and Et_4N^+ counter cation. The cross peaks (Fig. S11†) between H atoms on the alkyl chains of Et_4N^+ cations with aromatic rings of **MAA** in the ROESY spectrum of the host-guest mixture in DMSO-d_6 solution further confirmed the formation of the stable complex between **MAA** with F^- and Et_4N^+ ion-pairs. In fact, the electrostatic interaction between tetraethylammonium cation with F^- ions is the main
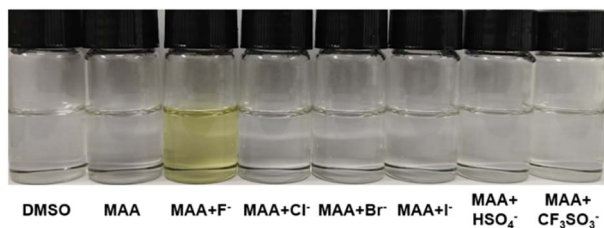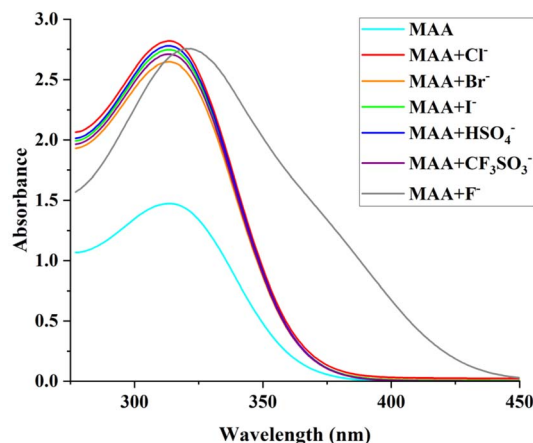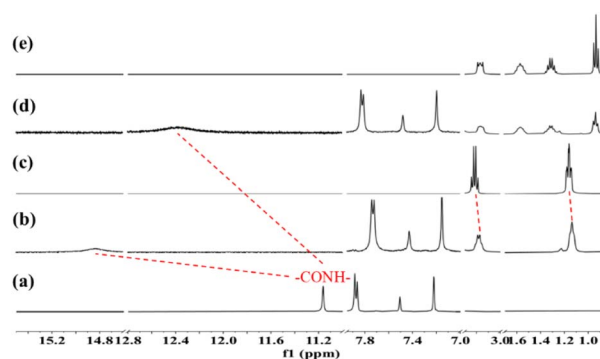

Fig. 3 Visible color changes of **MAA** observed before and after addition of equal amounts of various tetraethylammonium salts to DMSO solution (1.0 $\times 10^{-4}$ M): from left to right, DMSO, free **MAA**, **MAA** + F^-, **MAA** + Cl^-, **MAA** + Br^-, **MAA** + I^-, **MAA** + HSO_4^-, and **MAA** + $CF_3SO_3^-$.

Fig. 5 ^1H NMR (400 MHz, DMSO-d_6, 298 K) of (a) receptor **MAA**; (b) **MAA** + 5.0 equiv. of tetraethylammonium fluoride; (c) tetraethylammonium fluoride; (d) **MAA** + 5.0 equiv. of tetrabutylammonium fluoride; and (e) tetrabutylammonium fluoride.

driving force to bind Et_4N^+ ions in the cavity of the **MAA** receptor. In addition, the size matching effect of Et_4N^+ with the cavity of **MAA** is another factor to allow the binding of the guest ions.

Compared with Et_4N^+, the peaks of $n\text{-}Bu_4N^+$ showed almost no chemical shifts after mixing with **MAA** as shown in Fig. 5(d) and (e). This indicates that the oversized $n\text{-}Bu_4N^+$ is hard to bind into the macrocyclic cavity of **MAA**: it is much harder to fit into the cavity (and then only one can fit, with significant loss of entropy), and the C_4 alkyl chains does display their larger shielding of the positive charge on the central N atom, yields weaker interactions with the F^- anions (and thus with all proton's ^1H NMR shift is influenced by changes in the F^- binding). In addition, the smaller binding constants ($K_{a1} = 1.18 \times 10^3$ M and $K_{a2} = 2.32 \times 10^2$ M) between F^- and **MAA** in the presence of larger cation indicated that the association of cation in the cavity could facilitate the binding of F^- with the macrocycle.

DFT calculations

To further understand the spatial configuration of **MAA**, the binding mode of **MAA** with F^- ions and Et_4N^+ counter cation, and the source of its binding selectivity, we optimized the structures of **MAA** and its complexes with related ion-pairs by density functional theory (DFT) calculations at the B3LPY/6-31G level of theory using a PCM solvent model for DMSO. This yields the structures as shown in Fig. 6. From Fig. 6(a), it can be seen that macrocycle **MAA** presents a saddle-like planar structure in DMSO, which not only has a huge internal cavity (15.15 Å × 13.34 Å), but also displays three effective anion-binding sites due to the presence of the pyridine N atoms that made the hydrogen atoms of the two –(CO)NH– groups attached to it locked tightly inside the molecule, and thus tune these H atoms towards divalent binding of anions.

For the $2F^-$@**MAA** complex, the computationally optimized model was shown in Fig. S13,† the receptor **MAA** maintained a saddle-shaped steric structure upon binding to F^-. Within the molecule of the receptor **MAA**, there were not only strong N–H⋯F hydrogen bonds of lengths from 1.65 Å to 1.69 Å formed by the two –(CO)NH– groups and F^-, but also C–H⋯F weak hydrogen bonds of lengths from 2.14 Å to 2.36 Å formed by the benzene ring directly connected to the –(CO)NH– group and F^-. As can be seen in the optimized structures, F^- really fits in

the plane of the macrocyclic moiety that binds it, yielding strong interactions. In comparison, the complex of Cl^- with **MAA** was similarly yielding the structure shown in Fig. S14.† In this complex, Cl^- can only be bound above (or below) the plane of that moiety, and the H atoms of the –(CO)NH– groups have to bend outwards to interact optimally with the Cl^-. This size effect (Cl^- too big to fit, all other anions under study even bigger) clarifies why there is such selectivity towards binding fluoride anions.

The calculation also revealed further binding behavior of $2F^-$@**MAA** with counter cation. As shown in Fig. 6(b), the complex $2F^-$@**MAA** still possess a huge cavity which could easily fit an Et_4N^+. As expected, the cation bond into the cavity in a **MAA**–F^-–Et_4N^+ cascade form. In the optimized model, it is clearly that two or more Et_4N^+ cations could not fit in the rest cavity of **MAA** after binding F^- ions not only due to the size effect but also the strong electrostatic repulsion. In fact, the saddle-shape allows all two of the F^- to simultaneously interact with an Et_4N^+ cation, and thus form a relatively stable $[2F^-$@**MAA**$][Et_4N^+]$ complex. In this complex, the main driven force is the electrostatic attraction between the positively charged N atom and F^-. The model also showed that the multiple C–H⋯F hydrogen bonds (range from 2.14 to 2.19 Å) between the H atoms of alkyl chains in Et_4N^+ with F^-, and the C–H⋯π interactions between the alkyl chain H atoms with the aromatic rings (2.79 Å) of **MAA** play crucial roles to the formation of the quaternary complex. In this aspect, the formation of C–H⋯π interactions in the optimized model is in good agreement with the results of ROESY spectrum (Fig. S11†). According to these results, the binding of the counter cation Et_4N^+ partially counteracts the electrostatic repulsion between the two bonded fluoride ions, which further increased the binding strength and recognition selectivity between **MAA** and fluoride ions.

This changes for the much bigger and much more shielded $n\text{-}Bu_4N^+$ cation (Fig. S15†): to fit one $n\text{-}Bu_4N^+$ cation, the macrocycle the macrocyclic skeleton needs to undergo a very large distortion, noting that this would require a significant entropic penalty, but the overall electrostatic interactions are, of course, much weaker. Positioning two of such bulky Bu_4N^+ cations interacting with the $2F^-$@**MAA** structure requires them to move out considerably. As a result, the average electronic influence of $n\text{-}Bu_4N^+$ is much smaller than that of Et_4N^+, in line with experiment.

Conclusions

We designed and synthesized a 2,6-diamidopyridine-based macrocyclic aromatic amide receptor –– **MAA**, which combines a strong binding to fluoride anions with a high selectivity (very less binding to Cl^-, no binding to Br^-, I^-, HSO_4^-, and $CF_3SO_3^-$), which was confirmed by the ^1H NMR and UV-vis spectra. NMR titration experiments showed that **MAA** acts as a receptor to form a 1 : 2 complex with F^- in a large polar solvent, with binding constants of $K_{a1} = (1.47 \pm 0.4) \times 10^4$ M^{-1} and $K_{a2} = (7.15 \pm 0.51) \times 10^3$ M^{-1}, respectively. This complexation with F^- could be detected by the naked eye (color changes of DMSO solution from colorless to yellow). Importantly, **MAA** is
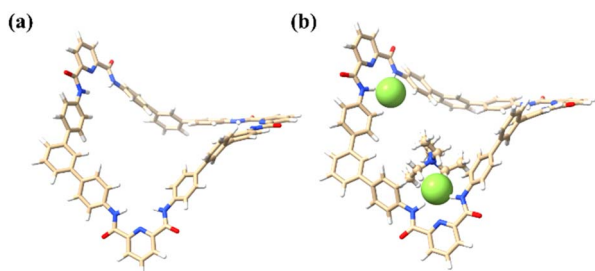

Fig. 6 The optimized structure of (a) **MAA** and (b) **MAA** + $2F^-$ + Et_4N^+ in DMSO.

also a cascade ion-pair recognition receptor without any cations binding sites in its macrocyclic structure. **MAA** could selectively host a Et$_4$N$^+$ rather than a larger n-Bu$_4$N$^+$ cation in the cavity after binding F$^-$ ions in the amide sites by the cascade **MAA**–F$^-$–Et$_4$N$^+$ pattern. The strong binding selectivity of **MAA** to F$^-$ and Et$_4$N$^+$ rather than other studied ions was also explained through using DFT calculations upon B3LYP/6-31G level.

Experimental section

General information

Unless otherwise stated, all reagents were obtained from commercial sources and were used without further purification. The solvents used were dried over 4A molecular sieves except for H$_2$O. ^{1}H NMR and ^{13}C NMR spectra were recorded on a Bruker DMX300 NMR and a Bruker® Avance III 400 MHz NMR spectrometer. HRMS was recorded on a Thermo Fisher. UV-vis absorption spectra were recorded on an Agilent Cary 7000 UV-vis-NIR spectrometer.

Synthesis

Synthesis of compound 1. 1,3-Dibromo-5-methoxybenzene (1.5 g, 5.64 mmol) and 4-(4,4,5,5-tetramethyl-1,3,2-dioxaborolan-2-yl)aniline (2.6 g, 11.87 mmol) were dissolved in 180 ml of a 1,4-dioxane/H$_2$O (5 : 1, v/v) solution system, then K$_2$CO$_3$ (4.67 g, 33.84 mmol) was added and heated to 100 °C in an argon atmosphere and the catalyst Pd(PPh$_3$)$_4$ (0.10 g, 0.09 mmol) was added and reacted for 12 h. At the end of the reaction the pH of the mixture was adjusted to weak acidity, water was added, and the organic solvent was removed under vacuum, then the organic layer was extracted with water and DCM and collected and dried with anhydrous MgSO$_4$. Purification by silica gel column chromatography (eluent: DCM/MeOH = 100/1 to DCM/MeOH = 50/1) afforded a yellow oily product **1** (1.41 g, yield 86.11%). ^{1}H NMR (400 MHz, DMSO-d_6) δ 7.44–7.38 (m, 4H), 7.23 (t, J = 1.6 Hz, 1H), 6.90 (d, J = 1.5 Hz, 2H), 6.66–6.60 (m, 4H), 5.23 (s, 4H), 3.83 (s, 3H). ^{13}C NMR (101 MHz, DMSO-d_6) δ 160.05, 148.37, 142.37, 127.62, 127.27, 115.27, 114.03, 108.44, 54.98. HRMS (ESI) for C$_{19}$H$_{18}$N$_2$O, m/z, [M + H]$^+$, calculated: 290.3660, found: 291.1491.

Synthesis of compound MAA. 2,6-Pyridinedicarboxylic acid (0.81 g, 4.86 mmol) and **1** (1.41 g, 4.86 mmol) were dissolved in THF (150 ml), EDC (2.79 g, 14.55 mmol) and HOBT (1.97 g, 14.55 mmol) were added and the reaction was heated to 65 °C and stirred the reaction for 4 h until the reaction reached equilibrium, then THF was removed in vacuum. Purification by silica gel column chromatography (eluent: EA/PE = 2/1 to EA/PE = 3/1, and DCM/MeOH = 50/1), followed by several recrystallizations using DCM and PE for further purification, afforded the white solid product **MAA** (0.10 g, 4.9%). ^{1}H NMR (400 MHz, DMSO-d_6) δ 11.16 (s, 1H), 8.45 (d, J = 7.7 Hz, 1H), 8.34 (dd, J = 8.5, 6.9 Hz, 1H), 8.03 (d, J = 8.4 Hz, 2H), 7.88 (d, J = 8.3 Hz, 2H), 7.22 (d, J = 1.4 Hz, 1H), 3.92 (s, 1H). ^{13}C NMR (101 MHz, DMSO-d_6) δ 161.90, 160.29, 148.97, 141.92, 137.65, 136.31, 134.17, 127.39, 125.36, 121.64, 118.74, 111.55, 55.46. HRMS (ESI) for

C$_{78}$H$_{57}$N$_9$O$_9$Na, m/z, [M + Na]$^+$, calculated: 1286.3572, found: 1286.4171.

Data availability

The data that support the findings of this study are available from the corresponding author, [Q. Shi], upon reasonable request.

Author contributions

X. Mao and Q. Shi did the synthesis work and the experiments of ^{1}H NMR, ^{13}C NMR, UV-vis spectra. R. Zhang did the HRMS experiments. X. Mao, Q. Shi, Y. Sun, and Q. Li written the manuscript. H. Zuilhof calculated the structures of receptor and its complexes. H. Zuilhof, L. Wang and X. Wang checked and revised the manuscript.

Conflicts of interest

There are no conflicts to declare.

Acknowledgements

References

1 Z. Liu, S. K. M. Nalluri and J. F. Stoddart, *Chem. Soc. Rev.*, 2017, **46**, 2459.

2 W. Zhang and J. S. Moore, *Angew. Chem., Int. Ed.*, 2006, **45**, 4416–4439.

3 L.-M. Bai, H. Yao, L.-P. Yang, W. Zhang and W. Jiang, *Chin. Chem. Lett.*, 2019, **30**, 881–884.

4 K. Jie, Y. Zhou, E. Li, R. Zhao and F. Huang, *Angew. Chem., Int. Ed.*, 2018, **57**, 12845.

5 T. Ogoshi, T. Yamagishi and Y. Nakamoto, *Chem. Rev.*, 2016, **116**, 7937–8002.

6 T. Ogoshi, T. Kakuta and T. Yamagishi, *Angew. Chem., Int. Ed.*, 2019, **58**, 2197–2206.

7 D. Cao, Y. Kou, J. Liang, Z. Chen, L. Wang and H. Meier, *Angew. Chem., Int. Ed.*, 2009, **48**, 9721.

8 X.-Y. Chen, H. Chen and J. F. Stoddart, *Angew. Chem., Int. Ed.*, 2023, **62**, e202211387.

9 S. Toyota and E. Tsurumaki, *Chem.–Eur. J.*, 2019, **25**, 6878–6890.

10 M. Yoshizawa and J. K. Klosterman, *Chem. Soc. Rev.*, 2014, **43**, 1885–1898.

11 Y.-D. Yang, X.-L. Chen, J.-L. Sessler and H.-Y. Gong, *J. Am. Chem. Soc.*, 2021, **143**, 2315.

12 M.-L. Tan, Q.-H. Guo, X.-Y. Wang, T.-H. Shi, Q. Zhang, S. K. Hou, S. Tong, J. S. You and M.-X. Wang, *Angew. Chem., Int. Ed.*, 2020, **59**, 23649.

13 A. J. McConnell and P. D. Beer, *Angew. Chem., Int. Ed.*, 2012, **51**, 5052–5061.

14 S. K. Kim and J. L. Sessler, *Chem. Soc. Rev.*, 2010, **39**, 3784–3809.

15 S. J. Nicholson, S. R. Barlow and N. H. Evans, *Chemistry*, 2023, **5**, 106–118.

16 A. J. McConnell, A. Docker and P. D. Beer, *ChemPlusChem*, 2020, **85**, 1824–1841.

17 Q. He, G. I. Vargas-Zúñiga, S. H. Kim, S. K. Kim and J. L. Sessler, *Chem. Rev.*, 2019, **119**, 9753–9835.

18 S. K. Kim, J. L. Sessler, D. E. Gross, C.-H. Lee, J. S. Kim, V. M. Lynch, L. H. Delmau and B. P. Hay, *J. Am. Chem. Soc.*, 2010, **132**, 5827–5836.

19 Q. He, G. M. Peters, V. M. Lynch and J. L. Sessler, *Angew. Chem., Int. Ed.*, 2017, **56**, 13396–13400.

20 D. Jagleniec, S. Siennicka, L. Dobrzycki, M. Karbarz and J. Romański, *Inorg. Chem.*, 2018, **57**, 12941–12952.

21 Q. He, Z. Zhang, J. T. Brewster, V. M. Lynch, S. K. Kim and J. L. Sessler, *J. Am. Chem. Soc.*, 2016, **138**, 9779–9782.

22 Q. He, N. J. Williams, J. H. Oh, V. M. Lynch, S. K. Kim, B. A. Moyer and J. L. Sessler, *Angew. Chem., Int. Ed.*, 2018, **57**, 11924–11928.

23 X. D. Chi, G. M. Peters, F. Hammel, C. Brockman and J. L. Sessler, *J. Am. Chem. Soc.*, 2017, **139**, 9124–9127.

24 P. Breccia, M. Van Gool, R. Pérez-Fernández, S. Martín-Santamaria, F. Gago, P. Prados and J. C. de Mendoza, *J. Am. Chem. Soc.*, 2003, **125**, 8270–8284.

25 X. L. Ni, X. Zeng, C. Redshaw and T. Yamato, *J. Org. Chem.*, 2011, **76**, 5696–5702.

26 D. S. Kim, V. M. Lynch, J. S. Park and J. L. Sessler, *J. Am. Chem. Soc.*, 2013, **135**, 14889–14894.

27 V. Valderrey, E. C. Escudero-Adan and P. Ballester, *Angew. Chem., Int. Ed.*, 2013, **52**, 6898–6902.

28 Z. Liu, Y. Zhou and L. Yuan, *Org. Biomol. Chem.*, 2022, **20**, 9023.

29 S. O. Kang, R. A. Begum and K. Bowman-James, *Angew. Chem., Int. Ed.*, 2006, **45**, 7882–7894.

30 M. A. Hossain, J. M. Llinares, D. Powell and K. Bowman-James, *Inorg. Chem.*, 2001, **40**, 2936–2937.

31 Q.-Q. Wang, R. A. Begum, V. W. Day and K. Bowman-James, *Inorg. Chem.*, 2012, **51**, 760–762.

32 J. Lohrman, H. Telikepalli, T. S. Johnson, T. A. Jackson, V. W. Day and K. Bowman-James, *Inorg. Chem.*, 2016, **55**, 5098–5100.

33 Q.-Q. Wang, V. W. Day and K. Bowman-James, *Org. Lett.*, 2014, **16**, 3982–3985.

34 S. O. Kang, D. Powell and K. Bowman-James, *J. Am. Chem. Soc.*, 2005, **127**, 13478–13479.

35 S. Xiong, M. V. N. Kishore, W. Zhou and Q. He, *Coord. Chem. Rev.*, 2022, **461**, 214480.

36 L. K. Macreadie, A. M. Gilchrist, D. A. McNaughton, W. G. Ryder, M. Fares and P. A. Gale, *Chem*, 2022, **8**, 46–118.

37 V. Amendola, G. Bergamaschi, M. Boiocchi, L. Fabbrizzi and L. Mosca, *J. Am. Chem. Soc.*, 2013, **135**, 6345–6355.